Systems/Circuits

Temporal Coding of Single Auditory Nerve Fibers Is Not Degraded in Aging Gerbils

Amarins N. Heeringa,* Lichun Zhang,* Go Ashida, Rainer Beutelmann, Friederike Steenken, and Christine Köppl
Cluster of Excellence "Hearing4all" and Research Centre Neurosensory Science, Department of Neuroscience, School of Medicine and Health Science, Carl von Ossietzky University Oldenburg, 26129 Oldenburg, Germany

People suffering from age-related hearing loss typically present with deficits in temporal processing tasks. Temporal processing deficits have also been shown in single-unit studies at the level of the auditory brainstem, midbrain, and cortex of aged animals. In this study, we explored whether temporal coding is already affected at the level of the input to the central auditory system. Single-unit auditory nerve fiber recordings were obtained from 41 Mongolian gerbils of either sex, divided between young, middle-aged, and old gerbils. Temporal coding quality was evaluated as vector strength in response to tones at best frequency, and by constructing shuffled and cross-stimulus autocorrelograms, and reverse correlations, from responses to 1 s noise bursts at 10–30 dB sensation level (dB above threshold). At comparable sensation levels, all measures showed that temporal coding was not altered in auditory nerve fibers of aging gerbils. Furthermore, both temporal fine structure and envelope coding remained unaffected. However, spontaneous rates were decreased in aging gerbils. Importantly, despite elevated pure tone thresholds, the frequency tuning of auditory nerve fibers was not affected. These results suggest that age-related temporal coding deficits arise more centrally, possibly due to a loss of auditory nerve fibers (or their peripheral synapses) but not due to qualitative changes in the responses of remaining auditory nerve fibers. The reduced spontaneous rate and elevated thresholds, but normal frequency tuning, of aged auditory nerve fibers can be explained by the well known reduction of endocochlear potential due to strial dysfunction in aged gerbils.

Key words: **age-related hearing loss; discharge rate; frequency tuning; presbycusis; stimulus envelope; temporal fine structure**

Significance Statement

As our society ages, age-related hearing deficits become ever more prevalent. Apart from decreased hearing sensitivity, elderly people often suffer from a reduced ability to communicate in daily settings, which is thought to be caused by known age-related deficits in auditory temporal processing. The current study demonstrated, using several different stimuli and analysis techniques, that these putative temporal processing deficits are not apparent in responses of single-unit auditory nerve fibers of quiet-aged gerbils. This suggests that age-related temporal processing deficits may develop more central to the auditory nerve, possibly due to a reduced population of active auditory nerve fibers, which will be of importance for the development of treatments for age-related hearing disorders.

Introduction

Age-related hearing loss is a highly common sensory disorder among elderly people. Approximately two-thirds of the population over seventy years old suffer from hearing problems, and the absolute numbers will only increase further as our society ages (Lin et al., 2011). People with age-related hearing loss face not only degraded hearing sensitivity, that is, elevated hearing thresholds, but also deficits in various temporal processing tasks (Plack et al., 2014; Ozmeral et al., 2016). These are typically evident in daily life as a reduced ability to communicate, resulting in social isolation, decreased quality of life, and even dementia in some severe cases (Strawbridge et al., 2000; Gurgel et al., 2014).

A variety of pathological changes within the cochlea are associated with age-related hearing deficits, and include degeneration of hair cells (*sensory presbyacusis*), neurons (*neural presbyacusis*), and stria vascularis (*strial presbyacusis*; Schuknecht and Gacek, 1993; Heeringa and Köppl, 2019). The quiet-aged Mongolian

Received Oct. 27, 2018; revised Oct. 25, 2019; accepted Nov. 4, 2019.

Author contributions: L.Z. and C.K. designed research; A.N.H., L.Z., and F.S. performed research; G.A. and R.B. contributed unpublished reagents/analytic tools; A.N.H. and L.Z. analyzed data; A.N.H., L.Z., G.A., R.B., F.S., and C.K. wrote the paper.

This work was supported by the DFG Cluster of Excellence EXC 1077/1 "Hearing4all". We thank Philip X. Joris from the K.U. Leuven for generously providing the code developed in his laboratory for the SAC/XAC analysis, and Amin Saremi and Helge Ahrens for providing technical assistance.

The authors declare no competing financial interests.

*A.N.H. and L.Z. contributed equally as co-first authors.

Correspondence should be addressed to Christine Köppl at christine.koeppl@uni-oldenburg.de.

https://doi.org/10.1523/JNEUROSCI.2784-18.2019

gerbil, a commonly used animal model for age-related hearing loss, typically presents with strial presbycusis. The cochlear lateral wall and stria vascularis are degenerated (Schulte and Schmiedt, 1992; Gratton et al., 1995), which results in a reduced endocochlear potential (EP; Schmiedt, 1996). Largely because of the dependence of outer hair-cell amplification on a high EP, loss of EP results in elevated hearing thresholds (Schmiedt, 1993; Schmiedt et al., 2002). Sensory presbycusis is more likely the result of otologic insults, such as exposure to loud noise or ototoxic compounds (Gates and Mills, 2005). Consistent with that, quiet-aged gerbils show only minimal inner hair-cell loss (Tarnowski et al., 1991). Recent studies have drawn attention to synaptopathy, which is a loss of ribbon synapses between inner hair cells and auditory nerve fibers (ANFs), as an ongoing effect of aging (Sergeyenko et al., 2013; Liberman and Kujawa, 2017). Functional consequences of synaptopathy are largely unclear and not detected by standard audiometric procedures (Kujawa and Liberman, 2015). Quiet-aged gerbils also show synapse loss toward the end of their lifespan (Gleich et al., 2016).

Studies addressing the effects of these age-related cochlear pathologies on coding of sounds in the auditory nerve at the single-unit level are scarce (Heeringa and Köppl, 2019). It has been shown in gerbils that rate-level functions are shifted toward higher levels, that is, have higher thresholds but are otherwise unaltered (Hellstrom and Schmiedt, 1991). Furthermore, a significant reduction of the number of low spontaneous rate (SR) fibers is encountered only among ANFs tuned to high frequencies (>6 kHz; Schmiedt et al., 1996). It is unknown whether temporal coding by ANFs is affected by age, as suggested from human psychophysical studies (Fitzgibbons and Gordon-Salant, 1996; Gordon-Salant et al., 2011).

ANFs temporally align their spiking activity to the phase of low frequencies in the acoustic signal, called phase locking. Phase locking faces a species-specific upper frequency limit (Heil and Peterson, 2017). Gerbil ANFs are able to phase lock to pure tones as high as 3 kHz (Versteegh et al., 2011). Temporal coding can be divided between coding of the envelope (ENV) and of the temporal fine structure (TFS), i.e., phase locking to the slow and fast amplitude fluctuations of the acoustic signal, respectively. Both TFS and ENV cues are important for speech understanding (Rosen, 1992). Low-pass filtered speech, containing only ENV information, can still be understood under quiet conditions (Shannon et al., 1995), while the TFS is critical for accurate perception of speech under degraded listening conditions (Hopkins and Moore, 2007; Swaminathan et al., 2016).

In this study, we aimed to understand whether phase locking and coding of TFS and ENV information is affected in ANFs of quiet-aged gerbils with age-related hearing loss. Furthermore, additional properties of spiking activity in the auditory nerve, including spontaneous and evoked firing rates, sharpness of tuning, and thresholds, were investigated.

Materials and Methods

Animals. Forty-one Mongolian gerbils (*Meriones unguiculatus*) of either sex (weight 51–103 g) were used in this study. Animals were divided into three groups: young animals (YO; age range 3–14 months, $n = 26$), middle-aged animals (MA; 23–33 months, $n = 6$), and old animals (OL; 37–42 months, $n = 9$). Experiments were conducted in a custom-built sound-attenuating chamber. Hearing thresholds were determined before surgery using auditory brainstem responses (ABRs) and were monitored at various time points throughout the experiment to assess the condition of the middle and inner ear. All animals were born at the University of Oldenburg animal house, raised and maintained in a controlled, quiet environment (average sound levels of 48 and 55 dB A outside and during working hours, respectively), and were free of middle-ear infections. All experimental procedures were approved by the ethics authorities of Lower Saxony, Germany (permit numbers AZ 33.9-42502-04-11/0337 and AZ 33.19-42502-04-15/1990).

Surgical preparation. Animals were anesthetized by intraperitoneal injection of a ketamine (135 mg/kg; Ketamin 10%, bela-pharm) and xylazine (6 mg/kg; Xylazin 2%, Ceva Tiergesundheit) mixture diluted in saline (0.9% NaCl). Anesthesia was maintained with subcutaneous injections of the same mixture containing one-third of the initial dose (45 mg/kg ketamine, 2 mg/kg xylazine) hourly or upon presence of a positive hindpaw reflex. In addition, a nonsteroidal antiphlogistic agent (meloxicam, 0.2 mg/kg) was injected at the beginning of the experiment, only when the animal was sensitive to the surgical procedures. The depth of anesthesia was constantly monitored by electrocardiogram recordings using intramuscular needle electrodes in the front leg and the contralateral hind leg, and by checking the absence of a muscle reflex upon a hindpaw pinch. Rectal body temperature was maintained at 38°C by a homeothermic blanket (Harvard Apparatus). To avoid airway obstruction during the experiment, middle-aged and old gerbils were tracheotomized but still breathed unaided. Some of the gerbils received additional oxygen (flow 1.5 L/min) in front of the tracheotomy or snout throughout the experiment. The head of the animal was fixed by using a bite bar, with the head mount, in addition, glued to the exposed frontal skull using dental cement (Kopf Instruments). After fixation of the head, the right pinna was removed to expose the bony ear canal. Subsequently, the ear bar, in which the speaker and the calibration microphone were sealed, was placed directly onto the bony ear canal. To avoid damage to the eardrum, the diameter of the ear bar's front end was a bit larger than the ear canal. The ear bar was sealed to the ear canal using petroleum jelly, to obtain a closed system from speaker to eardrum. A small opening was made in the bulla to prevent buildup of negative pressure in the middle ear.

To visualize the auditory nerve, a craniotomy of the right occipital bone was performed, followed by a duratomy and aspiration of cerebellar tissue until the brainstem and vestibular nerve were exposed. A few very small balls of paper tissue drenched in saline, with a maximal diameter <0.5 mm, were placed between the temporal bone and the brainstem to expose the auditory nerve. The auditory nerve could be discriminated from the cochlear nucleus using visual cues, including a distinct difference in color. To further ascertain that units were recorded from the ANF bundle, waveforms, response properties, and click delays were inspected carefully (see Data analysis).

Auditory brainstem responses. Two platinum needle electrodes (Grass Technologies) were placed subdermally: an active electrode ventral of the ear canal and a reference electrode in the neck close to the bulla to record ABRs evoked by chirps (see Acoustic stimuli to evoke auditory brainstem responses). The necessary surgeries did not leave any skin on the vertex to allow for a classical vertex placement of the reference electrode. ABRs were amplified (10,000 times) and bandpass filtered (0.3–3 kHz) using an amplifier (ISO 80, World Precision Instruments), and recorded using a Hammerfall DSP Multiface II (RME Audio; 48 kHz sampling rate) controlled by custom-written MATLAB software (MathWorks).

Acoustic stimuli to evoke auditory brainstem responses. Acoustic stimuli were generated and calibrated to the individual animal's ear using custom-written software in MATLAB and a Hammerfall DSP Multiface II. Stimuli were preamplified (HB7, TDT), and presented through a small speaker (ER-2, Etymotic Research, or IE 800, Sennheiser) that was sealed into the ear bar. Stimuli were calibrated after each placement of the ear bar by measuring SPL near the eardrum with a miniature microphone (FG-23329, Knowles Electronics, or ER7-C, Etymotic Research in combination with the ER-2 or IE 800 speaker, respectively) sealed in the same ear bar, amplified by a microphone amplifier (MA3, TDT). ABRs were measured during the presentation of custom-generated chirps to compensate for the frequency-dependent group delays along the gerbil cochlea (Dau et al., 2000; Versteegh et al., 2011; 0.3–19 kHz, 4.2 ms duration). Stimulus levels were typically separated by 5 dB and were presented randomly (300–500 repetitions). ABR thresholds were visually defined, as the lowest sound level at which clear ABR waves were still distinguishable.

Auditory-nerve single-unit recordings. Single units in the ANF bundle were recorded using glass micropipette electrodes (GB120F-10, Science Products; pulled using a P-2000, Sutter Instruments), filled with a 3M-KCl solution and impedances typically between 10 and 60 MΩ. Electrodes were placed just above the ANF bundle under visual control with a micromanipulator and then advanced remotely via a piezo microdriver (6000 ULN inchworm motor controller and 6005 ULN handset, Burleigh). Neural signals were amplified (WPI 767, World Precision Instruments), filtered for line frequency noise (50/60 Hz; Hum Bug, Quest Scientific), played over a speaker (MS2, TDT), visualized on an oscilloscope (SDS 1102CNL, SIGLENT Technologies), and digitized (RX6, TDT; 48,828 Hz sampling rate) before storage on a personal computer using custom-written MATLAB software. Spike triggering was defined interactively during the experiment and was more carefully manually revisited offline on a trial-by-trial basis (see Data analysis).

Acoustic stimuli for single-unit recordings. As the glass electrode was advanced through the ANF bundle, a broadband noise search stimulus was presented (1–9 kHz, 50–70 dB SPL) until a single unit was isolated, as judged on the oscilloscope by spike amplitude and interspike interval. After a quick audiovisual estimate of the fiber's sensitive range, best frequency (BF) was determined by recording neural responses to tone bursts at ~10 dB above threshold (range 0–30 dB above threshold, 50 ms duration, including 5 ms cosine rise/fall times, 5–10 repetitions). Next, tone bursts at BF (50 ms duration, 5 ms rise/fall time, 10 repetitions) were presented at levels ranging from 10 to 79 dB SPL (3 dB step size) to derive a rate-level function and determine the unit's threshold. If the fiber had a BF < 10 kHz, more repetitions of tone bursts at BF (50 ms duration, 5 ms rise/fall time, 40 repetitions) were presented at several levels below and above threshold (10 dB step size), to test for phase locking. To estimate temporal coding in response to noise, a stimulus consisting of two 1 s noise bursts (separated by 200 ms, 10 ms cosine ramps, 60 repetitions) was presented at 10–30 dB above the unit's threshold. Noise bursts had a frequency range of 0.2–12 kHz and were identical between repetitions (frozen noise). The second burst of each stimulus pair was 180° phase inverted relative to the first (Joris, 2003; Louage et al., 2004). Noise bursts were filtered to compensate for the frequency response of the hardware, according to the individual ear's calibration. If the unit was still stably isolated, pure tones from a matrix of a broader range of frequencies (100–250 Hz step size) and levels (3–5 dB step size, 50 ms durations, 5 ms rise/fall time, 5 repetitions) were presented randomly, to determine the receptive field and derive a tuning curve, and 80 dB clicks were presented (5 ms delay, 20 ms acquisition time, condensation click, 500 repetitions) to determine response latency. All stimuli were calibrated before presentation according to the latest calibration. A new calibration was obtained after each new placement of the ear bar, using a miniature microphone (either the FG-23329, Knowles Electronics, or the ER7-C, Etymotic Research) sealed near the speaker in the same ear bar, a microphone amplifier (MA3, TDT; set at 40 dB amplification), and custom-made MATLAB software.

Data analysis. As our testing protocols were quite prolonged, typically >30 min if all recordings were acquired, spike amplitude could vary within and between single recordings. Therefore, threshold for spike detection was set offline for each individual trial using custom-written MATLAB software. Single-unit isolation was confirmed by checking the interspike intervals, of which a large majority should be >1 ms and none should be <0.6 ms based on the absolute ANF refractoriness (Heil et al., 2007). Recordings from 16 of a total of 463 units were excluded based on this criterion. Furthermore, spike waveforms were carefully inspected to exclude the presence of a pre-potential, which would indicate that the unit was recorded from the ventral cochlear nucleus instead of from the ANF bundle (Keine and Rübsamen, 2015). There were no units recorded in which a pre-potential was observed. In addition, when responses to clicks were recorded, a click latency <2 ms gave an additional confirmation that the unit was recorded from the ANF bundle (FitzGerald et al., 2001). The click latency was determined by two consecutive bins (0.05 ms) in the peristimulus time histogram (PSTH) being higher than the highest bin before the onset of the click (spontaneous rate). Three units were excluded based on having a click latency that was unlikely to be derived from the auditory nerve. Last, the shape of the PSTH at 20 and 30 dB above threshold and the shape of the rate-level function to BF tones were inspected. Three additional units were excluded based on non-primary like PSTH (e.g., chopper) or rate-level function (e.g., non-monotonic).

To determine BF, mean spike rates in responses to tone bursts at a fixed level of ~10 dB above threshold were fitted using a smoothing spline and the frequency at which the fitted line reached maximum firing rate was defined as BF. Bandwidth of the frequency-response curve was determined at the half-maximum evoked rate (relative to mean SR) from the fitted function only from recordings that were collected at a level between 5 and 15 dB above threshold. Threshold was determined from the rate-level function, defined as the tone level evoking a firing rate larger than the SR + 2.5 × SD of the SR and at least 15 spikes/s above the SR. Characteristic frequency (CF) and threshold were also determined from the threshold-tuning curve that could be interpolated from the receptive field, whenever these data were recorded (see Fig. 8*A*). These values were used as BF and threshold when data from the rate-frequency and rate-level curve were unavailable (in $n = 6$ and $n = 4$ units, respectively). Furthermore, the $Q_{10\,dB}$ value was derived from the tuning curve, which is calculated by dividing CF by the tuning-curve bandwidth at 10 dB above threshold. SRs were calculated from randomly presented silent trials throughout the tone presentations. Noise-evoked firing rates were calculated from responses to both noise bursts.

To determine temporal coding in response to pure tones, the vector strength (VS) was calculated (Goldberg and Brown, 1969), which represents the tendency of a unit to phase lock to the period of the tone:

$$VS = \frac{1}{N}\left|\sum_{j=1}^{N} e^{i\varphi(j)}\right|,$$

where N represents the total number of spikes and $\varphi(j)$ is the phase of the jth spike relative to the period of the tone. A p value of the VS was calculated by $p = e\text{^}(-N \times VS^2)$, where $p < 0.001$ and $N > 50$, was considered a significant VS (Mardia and Jupp, 2000).

More extensive temporal coding properties of single units were determined by analyzing responses to the noise bursts. Noise-evoked responses of units were analyzed only when >25 repetitions and >1000 noise-evoked spikes were recorded. Shuffled autocorrelograms (SACs) and cross-stimulus autocorrelograms (XACs) were constructed using a bin width of 20 μs, according to procedures established by Joris (2003) and Louage et al. (2004). SACs and XACs were normalized for firing rate, number of repetitions, bin width, and stimulus duration. The ratio between the XAC and the SAC at $t = 0$ ms delay was calculated, which represents a metric for the transition from predominantly TFS to predominantly ENV phase locking. Subsequently, the DifCor was calculated by a bin per bin subtraction of the XAC from the SAC, and the SumCor was calculated by taking the bin per bin average of the SAC and the XAC. Leakage of locking to the TFS into the SumCor was minimized by applying a low-pass Chebyshev filter (6th order, type II, 30 dB stopband ripple attenuation) with a cutoff frequency at the BF of the unit (Heinz and Swaminathan, 2009). The peak height of the DifCor and the SumCor was used as a measure for temporal coding of the TFS and the ENV, respectively, whereas the peak width of the DifCor and SumCor represents temporal precision (jitter) of the phase locking (Louage et al., 2004). Units in which the SAC peak height (correlation index) was not significant for either of the two noise bursts, as determined by a bootstrap method on random permutations of the interspike intervals ($p > 0.01$; Joris et al., 2006), were excluded from the XAC/SAC ratio, DifCor, and SumCor analyses.

Responses to the noise bursts, subjected to the same inclusion criteria as for the SAC/XAC analysis, were also used to calculate the reverse correlation (*revcor*; de Boer and Kuyper, 1968; de Boer and de Jongh, 1978). The *revcor* function equals the cross-correlation of the acoustical input and the neural spike signal, and is proportional to the normalized average noise stimulus preceding the spikes. Oscillations in the *revcor* function appear when the unit phase locks to a frequency within its receptive field that is present in the noise stimulus (see Fig. 3*A*). The noise that was presented at the eardrum of the gerbil was reconstructed by

reversing the compensation that was applied to the noise to account for the frequency response of the hardware. Unfortunately, it turned out *post hoc* that not all calibrations had been correctly performed and applied to the noises. However, the system response typically did not vary more than ± 5 dB in the 0.5–3.5 kHz frequency range, the frequency range of interest for temporal coding of the TFS. After carefully going over the data, unit responses from one young animal were excluded from the *revcor* analysis based on outlying noise properties that could not be corrected for. Because the absolute amplitude of the noise differed depending on the threshold of the unit, the noise that was used to calculate the *revcor* was normalized to have an RMS value of 1. Subsequently, the *revcor* function was calculated as follows:

$$revcor(\tau) = \frac{1}{N}\sum_{i=1}^{N} x(t_i - \tau),$$

in which τ is the time before the spike, $x(t)$ is the normalized input noise signal, N is the total number of spikes, and t_i (with $i = 1,\ldots,N$) are the spike times. Oscillations in the *revcor* were considered significant if the maximal *revcor* amplitude exceeded five times the RMS of the *revcor* function, calculated from a time window where no significant oscillations were expected (between $t = -20$ ms and $t = -8$ ms relative to t_i). If the *revcor* was significant, the magnitude of the highest spectral peak was used as an additional measure to quantify temporal coding (see Fig. 3*B*). The *revcor* spectrum was also used to determine the *revcor* frequency (at highest spectral peak) and the 10 dB filter bandwidth, which is very similar to the unit's tuning curve (de Boer and de Jongh, 1978).

Experimental design and statistical analysis. Differences between measures of young, middle-aged, and old gerbils were tested for significance preferentially with the nonparametric Kruskal–Wallis test, followed by pairwise comparisons using the Mann–Whitney *U* test. If assumptions of normality were not violated, the ANOVA and *post hoc* Tukey–Kramer's test were used. Metrics that typically varied as a function of BF were tested for significance using an analysis of covariance (ANCOVA), with BF as the covariate. Significant correlations were detected using the nonparametric Spearman's rank test. *P* values were Holm–Bonferroni corrected for multiple comparisons. All statistical tests were done in MATLAB (R2017b) using the Statistics and Machine Learning Toolbox v11.2. The criterion *p* value for significance was conservatively chosen at 0.01. For analyses with inconclusive results (null hypothesis retained) that were of critical importance, power analyses were performed based on the sample and effect sizes actually observed, using $\alpha = 0.01$ and taking the covariate BF into account when necessary. The power calculations were performed with the PASS Software v16.0.4 (PASS 16 Power Analysis and Sample Size Software, 2018, NCSS).

Results

Gerbils were divided into three age groups: YO (3–14 months, $n = 26$), MA (23–33 months, $n = 6$), and OL (37–42 months, $n = 9$).

Old gerbils exhibited variable hearing loss

Overall hearing sensitivity was determined using ABRs evoked by chirps. Middle-aged and old gerbils had significantly higher thresholds than young gerbils but did not significantly differ from each other (Kruskal–Wallis test: $H_{(2)} = 21.69$, $p = 1.95 \times 10^{-5}$; Mann–Whitney *U* tests: YO vs MA, $p = 1.60 \times 10^{-3}$, YO vs OL, $p = 1.50 \times 10^{-4}$, MA vs OL, $p = 0.23$). The median threshold shifts of the middle-aged and old animals were 25 and 40 dB, respectively (Fig. 1*A*). Furthermore, there was substantial variation in the threshold shift among old gerbils (range 10–55 dB relative to the median threshold of young gerbils), suggesting that not all old gerbils experienced the same amount of age-related hearing loss. Plotting individual threshold against the animal's age confirmed that, although there is a general effect of age on hearing threshold, the variation increases with age as well (Fig. 1*B*).

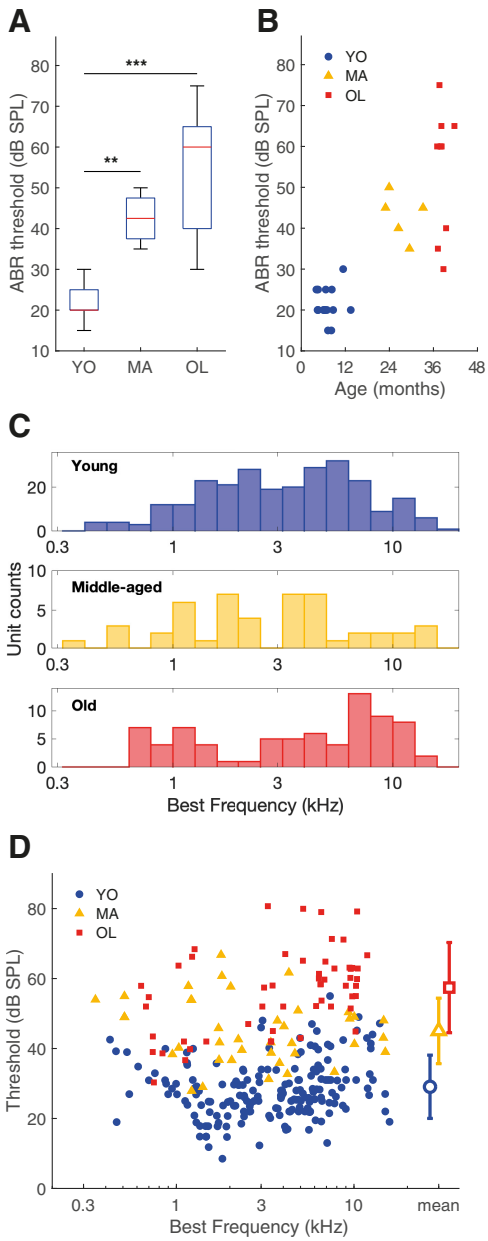

Figure 1. Quiet-aged gerbils presented variable degrees of age-related hearing loss. ***A***, Box plots of ABR thresholds elicited by chirps in YO ($n = 15$), MA ($n = 5$), and OL ($n = 9$) gerbils. Stars indicate a significant difference between two groups after *post hoc* comparisons. $^{**}p < 0.01$, $^{***}p < 0.001$, Bonferroni–Holm corrected. Box plots show the median (horizontal red line), 25th and 75th percentile (blue box), and more extreme data points not considered outliers (whiskers). Data points are considered outliers if they are higher than the 75th percentile + 1.5 × (75–25th percentile) or lower than the 25th percentile–1.5 × (75–25th percentile), which approximates ±2.7 × SD. For the ABR thresholds of the young gerbils, the median and 25th percentiles are the same value and are therefore on top of each other. ***B***, The ABR threshold to chirps of each animal, as a function of its age in months. ***C***, The BF distribution of all auditory nerve single units recorded from young animals ($n = 261$, blue), middle-aged animals ($n = 48$, yellow), and old ($n = 76$, red) animals. ***D***, Threshold as a function of the fiber's BF in young (blue circles; $n = 186$), middle-aged (yellow triangles; $n = 39$), and old (red squares; $n = 54$) animals. Mean thresholds ± SD are shown with large open symbols on the right.

The BF distribution of recorded auditory-nerve single units is shown for each group in Figure 1*C* and showed evidence of bimodality, particularly in the young and old group. A bimodal BF distribution with a notch near 3.5 kHz is typical for the gerbil

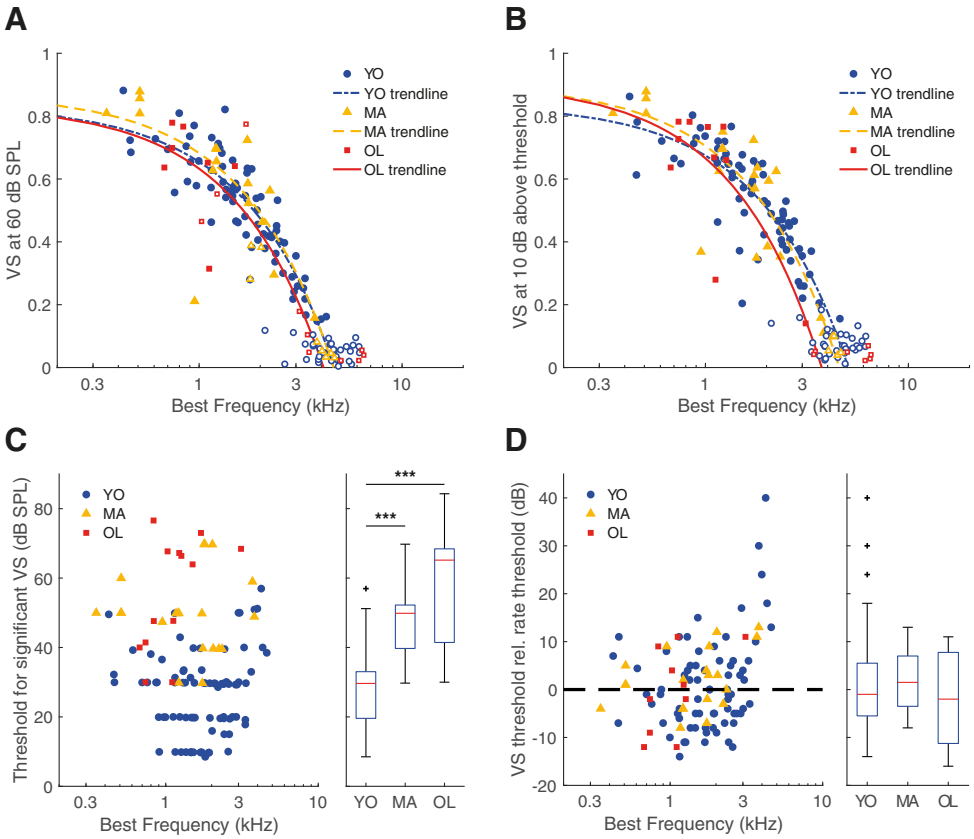

Figure 2. Phase locking to pure tones was not affected by aging. ***A***, VS of the units' response to a BF tone at 60 dB SPL, as a function of BF, for young ($n = 74$), middle-aged ($n = 16$), and old ($n = 7$) gerbils. Open symbols indicate VS values that were not significant ($p > 0.001$ or $N < 50$; see Materials and Methods), which were not included in the analysis. The few high, yet nonsignificant VS values in the middle-aged and old gerbil group come from units with a high threshold and thus a small number of spikes ($N < 50$). VS values from units with a firing rate <5 spikes/s at 60 dB SPL are not shown (MA: $n = 1$, OL: $n = 5$). The trend lines show linear regressions, separately for young, middle-aged, and old gerbils (note the logarithmic scale of the horizontal axis). ***B***, Same format as in ***A***, but here VS is examined for BF tones at 10 dB above threshold (YO: $n = 69$, MA: $n = 20$, OL: $n = 10$). ***C***, The lowest sound level where VS was significant, as a function of BF. To the right, the population data are presented as a box plot in the same format as in Figure 1*A* (YO: $n = 86$, MA: $n = 20$, OL: $n = 13$). Outliers are presented as black crosses. ***D***, Same format as in ***C*** but VS threshold is now shown relative to the rate threshold (VS threshold − rate threshold; YO: $n = 73$, MA: $n = 20$, OL: $n = 10$). The dotted reference line indicates where the VS threshold is equal to the rate threshold, data points below this line represent significant phase locking at sound levels that did not elicit a significant increase in firing rate. In all panels, blue circles indicate data from young gerbils, yellow triangles from middle-aged gerbils, and red squares from old gerbils. ***$p < 0.001$. Outliers are presented as black crosses (+).

auditory nerve (Huet et al., 2016). Thresholds to BF tone bursts differed significantly with age (one-way ANOVA: $F_{(2)} = 194$, $p = 3.81 \times 10^{-54}$). Single-unit thresholds of middle-aged gerbils had a significant mean elevation of 16 dB relative to the mean threshold of young animals [95% confidence interval (CI): 12–20 dB difference, Tukey–Kramer's test: $p = 9.56 \times 10^{-10}$]; thresholds of old gerbils were elevated by 28 dB relative to controls (95% CI: 25–32 dB difference, Tukey–Kramer's test: $p = 9.56 \times 10^{-10}$). At the single-unit level, thresholds differed also significantly between the middle-aged and the old group (mean elevation: 12 dB; 95% CI: 8–17 dB; Tukey–Kramer's test: $p = 7.51 \times 10^{-9}$; Fig. 1*D*).

Phase locking to pure tones was not altered with age

Temporal coding in ANFs was studied using various measures. First, VS, a measure for synchronization to the period of a BF tone, i.e., TFS coding, was studied at different sound levels. Figure 2*A* shows VS of young, middle-aged, and old gerbils in response to BF tones of a fixed level (60 dB SPL). Analysis of covariance did not reveal a significant difference in VS between age groups (effect of group, $F_{(2)} = 0.58$, $p = 0.56$; estimated power = 80%; Fig. 2*A*). Because rate thresholds between age groups differed significantly (Fig. 1*D*) and VS varies as a function of level relative to threshold (Huet et al., 2018), we also compared VS at a fixed sensation level (10 dB above the individual unit's rate threshold). At this level, VS also did not differ between the age groups (ANCOVA: effect of group, $F_{(2)} = 0.48$, $p = 0.62$; Fig. 2*B*). Here, the estimated test power was low (17%), however the differences between the trendlines were small and unsystematic (effect size (Cohen's f) = 0.09). Next, we determined the lowest sound level at which the VS was significant ($p < 0.001$), which was termed the VS threshold. VS thresholds were significantly higher in middle-aged and old gerbils than in young gerbils, with median elevations of 20 and 36 dB, respectively (Kruskal–Wallis test: $H_{(2)} = 51.26$, $p = 7.40 \times 10^{-12}$; Mann–Whitney *U* tests: YO vs MA, $p = 3.82 \times 10^{-8}$, YO vs OL, $p = 4.84 \times 10^{-7}$, MA vs OL, $p = 0.23$; Fig. 2*C*). However, this threshold is conceivably confounded by the rate threshold. Therefore, we calculated the VS threshold relative to the rate threshold. A negative value means that significant phase locking to the tone was present at a level where no significant rate change was yet observed. This relative threshold did not differ significantly between the age groups (Kruskal–Wallis test: $H_{(2)} = 1.75$, $p = 0.42$; Fig. 2*D*). Together, these results show that the absolute sound level at which significant phase locking emerges in ANFs was increased in middle-aged and old gerbils, further indicative of age-related hearing loss, whereas the qualitative properties of phase locking to BF tones in quiet did not differ with increasing age.

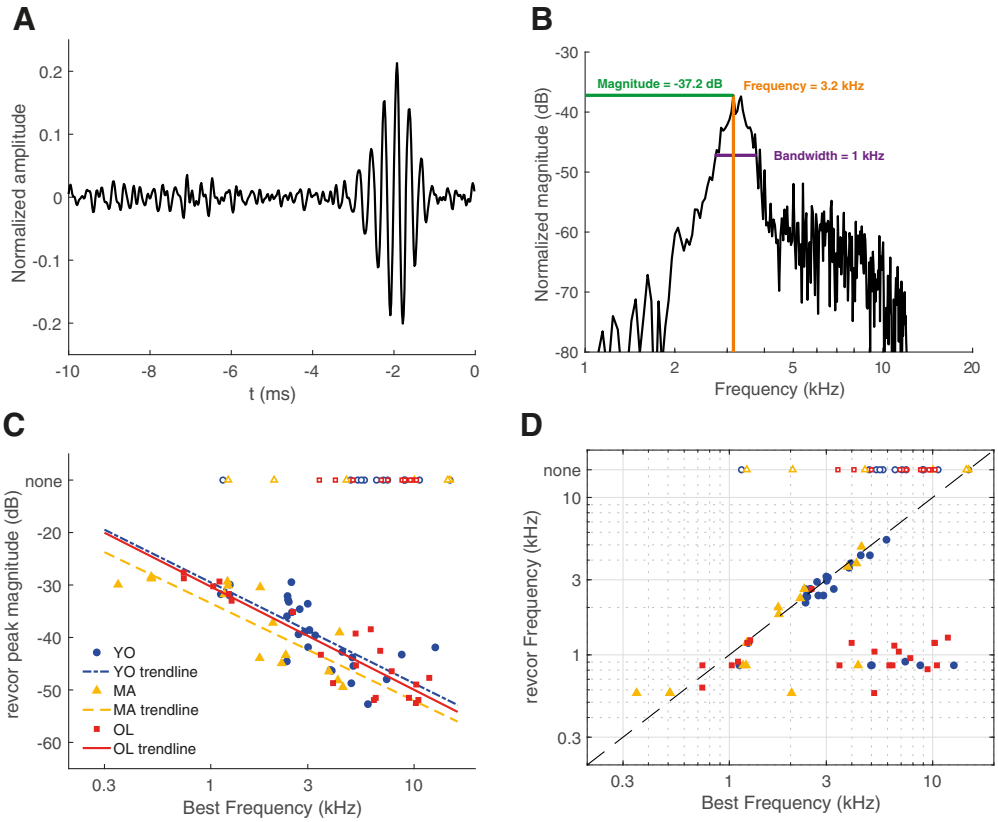

Figure 3. Temporal coding measures derived from the revcor were not affected by aging. ***A***, An example of a *revcor*, with a significant oscillation occurring ~−2 ms relative to the spike (t = 0 ms). BF of this unit was 3.0 kHz. ***B***, Spectrum of the *revcor* function shown in ***A***. Peak magnitude, *revcor* frequency at peak magnitude, and bandwidth at 10 dB below peak magnitude are indicated in the plot. ***C***, *Revcor* peak magnitude as a function of BF for young (blue circles), middle-aged (yellow triangles), and old gerbils (red squares). Magnitudes were similar between groups but decreased with increasing BF. Logarithmic regression lines are shown as visual aids, separately for the different groups (YO: n = 27, MA: n = 15, OL: n = 21). ***D***, *Revcor* frequency as a function of BF for young, middle-aged, and old gerbils. The dashed line represents $y = x$. Open symbols at the top of the graph in ***C*** and ***D*** indicate the BF of units that had no significant *revcor* oscillation (none).

Peak magnitude of the reverse correlation was not affected by aging

Single-unit responses to noise bursts were analyzed using a *revcor* paradigm, which shows a significant oscillation when the unit phase locks to a frequency present in the noise stimulus, typically its BF. The *revcor* can be considered to represent the normalized average stimulus that elicited a spike, with t = 0 ms indicating the time of the spike. An example of a *revcor* from a unit of a young gerbil is shown in Figure 3*A*. The frequency to which the unit responded (3.2 kHz) can be derived from the spectrum of the *revcor* and was close to its BF at 3.0 kHz (Fig. 3*B*). The peak magnitude in the *revcor* spectrum is considered a measure for robustness of temporal coding of the TFS (analogous to VS and DifCor peak height). For a given ANF unit, *revcor* magnitude typically decreases with increasing sound level (Recio-Spinoso et al., 2005). The levels of the noise stimuli were therefore selected following online sensitivity measures during the experiment, aiming for similar sensation levels between units (between 10–30 dB above threshold). Indeed, noise-evoked firing rates did not differ between the different age groups (Kruskal–Wallis test: $H_{(2)}$ = 3.83, p = 0.15; YO: n = 39, MA: n = 21, OL: n = 31). Average absolute noise levels were 53.6, 66.2, and 79.7 dB SPL for the young, middle-aged, and old gerbils, respectively, and these did differ significantly between the groups (Kruskal–Wallis test: $H_{(2)}$ = 52.18, $p = 4.94 \times 10^{-12}$), which mirrors the increased thresholds in the middle-aged and old gerbils (Fig. 1*D*).

Strength of temporal coding of the TFS clearly decreased with increasing BF and there was no significant difference in *revcor* magnitude between the different age groups when controlling for BF (ANCOVA: effect of group, $F_{(2)}$ = 3.43, p = 0.04; Fig. 3*C*). Although the estimated test power was low (11%), the observed effects were so small (effect size = 0.1) that we would not consider them biologically relevant even if a much larger sample showed them to be statistically significant. Plotting the *revcor* frequency against the unit's BF showed that most units with a BF <3.5 kHz had a *revcor* frequency similar to BF (Fig. 3*D*). Note that some units with a BF > 3.5 kHz still showed a significant *revcor*, but the *revcor* frequency was considerably lower, suggesting that they phase locked to frequencies far below BF (~1 kHz). This is a well known phenomenon in mammalian ANFs if the stimulus level is high enough to excite units at frequencies in the tail regions of their frequency-threshold curves (Heil and Peterson, 2017). Units from gerbils of all age groups showed a similar correspondence between BF and *revcor* frequency and a similar incidence of insignificant *revcors* (43%, 40%, and 45% for young, middle-aged, and old gerbils, respectively).

TFS and ENV coding, at comparable sensation levels, were unaffected by aging

To study temporal coding more in depth and to be able to distinguish TFS coding from ENV coding, responses to noise bursts were also analyzed by constructing SACs from responses to different trials of the same noise bursts and XACs from responses to trials of noise bursts of opposite polarity (Louage et al., 2004). A total of six units (YO: n = 1/39, MA: n = 2/19, OL: n = 3/29) did not show any locking to either TFS or ENV, as determined by a

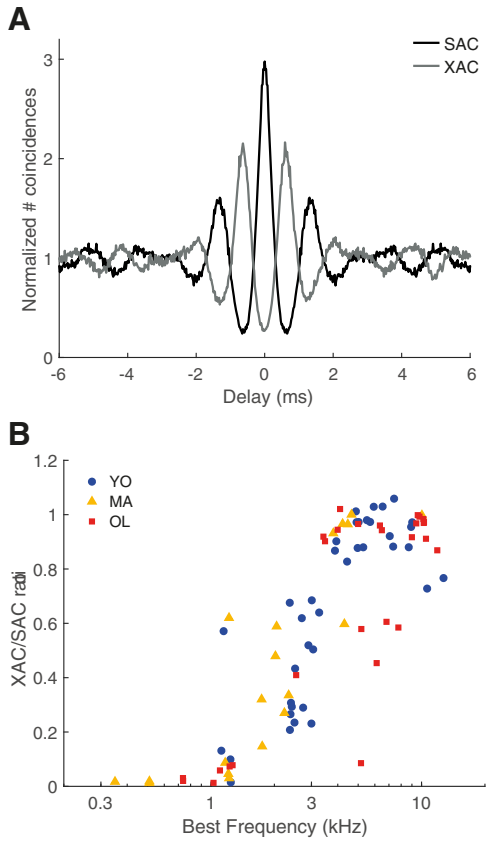

Figure 4. Transition from predominantly fine structure coding to predominantly envelope coding with increasing BF. ***A***, Example of the SAC (black line) and XAC (gray line) of noise responses from a unit of a young gerbil (BF = 900 Hz). The XAC/SAC ratio at 0 ms delay of this unit was 0.09. ***B***, The XAC/SAC ratio at delay = 0 ms, as a function of BF for young (blue circles), middle-aged (yellow triangles), and old gerbils (red squares).

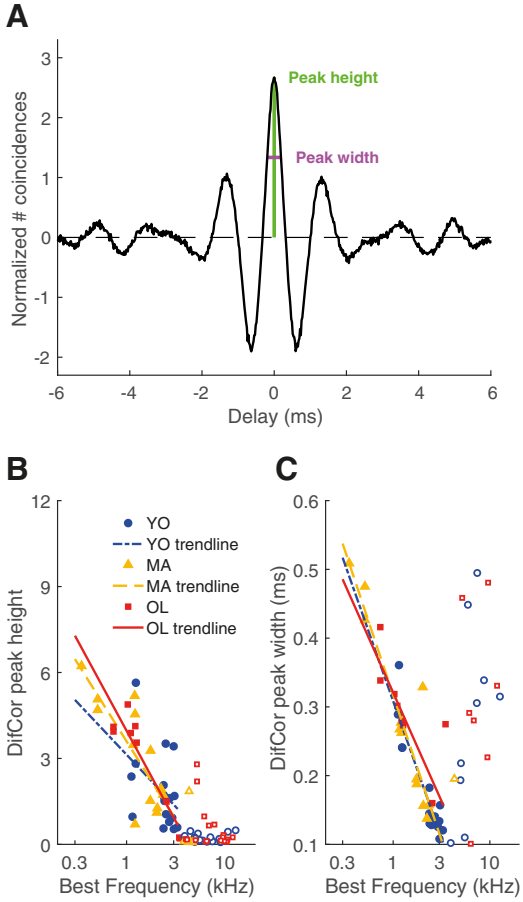

Figure 5. DifCor peak height and width were not affected by aging. ***A***, Example of the DifCor, for the same unit shown in Figure 4*A*. Peak height (at delay = 0 ms, from dotted reference line) was 2.67 (represented in green) and peak width was 0.38 ms (represented in magenta). ***B***, DifCor peak height as a function of BF for young (blue circles; $n = 18$), middle-aged (yellow triangles; $n = 13$), and old gerbils (red squares; $n = 9$). Peak heights were similar between the different age groups, but decreased with increasing BF. Logarithmic regressions are shown as visual aids. Open symbols in ***B*** and ***C*** indicate units with a BF > 3.5 kHz and were not included in the regression analyses. ***C***, Same data and format as in ***B*** but now plotting DifCor peak width.

bootstrap method on interspike intervals on the SAC (Joris et al., 2006), and were therefore not included in subsequent analyses. Figure 4*A* depicts an example of the SAC (black) and XAC (gray) from one unit of a young gerbil (BF = 0.9 kHz). The ratio between the XAC and the SAC at delay = 0 ms was calculated to determine whether the fiber was predominantly locking to the TFS or to the ENV of the stimulus. All included units with a BF < 3.5 kHz showed XAC/SAC ratios <0.7 (Fig. 4*B*) and were thus primarily phase locking to the TFS (Fig. 4*A*). In contrast, units with a BF > 3.5 kHz generally showed high XAC/SAC ratios and were thus primarily phase locking to the ENV of the stimulus, consistent with previous data by Louage et al. (2004).

The DifCor was calculated by subtracting the XAC from the SAC, and displays regular oscillations separated by ~half the period of BF if the unit phase locked to the TFS of the acoustic signal (Fig. 5*A* shows an example of the DifCor derived from the SAC and XAC in Fig. 4*A*). DifCor peak height is then a measure of the strength of phase locking to the TFS (analogous to VS and *revcor* peak magnitude) and DifCor peak width represents the amount of spike jitter of phase locking. DifCor peak height did not differ between young, middle-aged, and old gerbils when controlling for BF (ANCOVA: effect of group, $F_{(2)} = 0.102$, $p = 0.90$; estimated power = 74%; Fig. 5*B*). DifCor peak width also did not differ between the different age groups (ANCOVA: effect of group, $F_{(2)} = 1.14$, $p = 0.33$; Fig. 5*C*). Because the high-frequency units with a XAC/SAC ratio <0.7 likely showed TFS phase locking to tail frequencies of their tuning curve (see previous section; Fig. 3*D*), only fibers with a BF < 3.5 kHz were included in the statistical analyses of the DifCor (Fig. 5*B*,*C*, filled symbols).

The SumCor was calculated by taking the average of the XAC and SAC and shows a simple peak if the unit locked to ENV features of the acoustic signal (Fig. 6*A*). The SumCor peak height, representing strength of ENV coding, did not vary with BF [ANCOVA: effect of group, $F_{(2)} = 0.07$, $p = 0.93$; effect of log(BF), $F_{(2)} = 0.35$, $p = 0.56$; Fig. 6*B*] and were therefore further analyzed with the Kruskal–Wallis test. This showed no significant effect of age on SumCor peak height (Kruskal–Wallis test: $H_{(2)} = 1.92$, $p = 0.38$; Fig. 6*B*). The estimated test power was very low (<10%) but, again, the observed differences between age groups were extremely small and probably not biologically relevant. Likewise, the SumCor peak width, representing the jitter of ENV coding, showed only minimal, insignificant differences between young, middle-aged, and old gerbils (ANCOVA: effect of group, $F_{(2)} = 1.05$, $p = 0.35$; Fig. 6*C*).

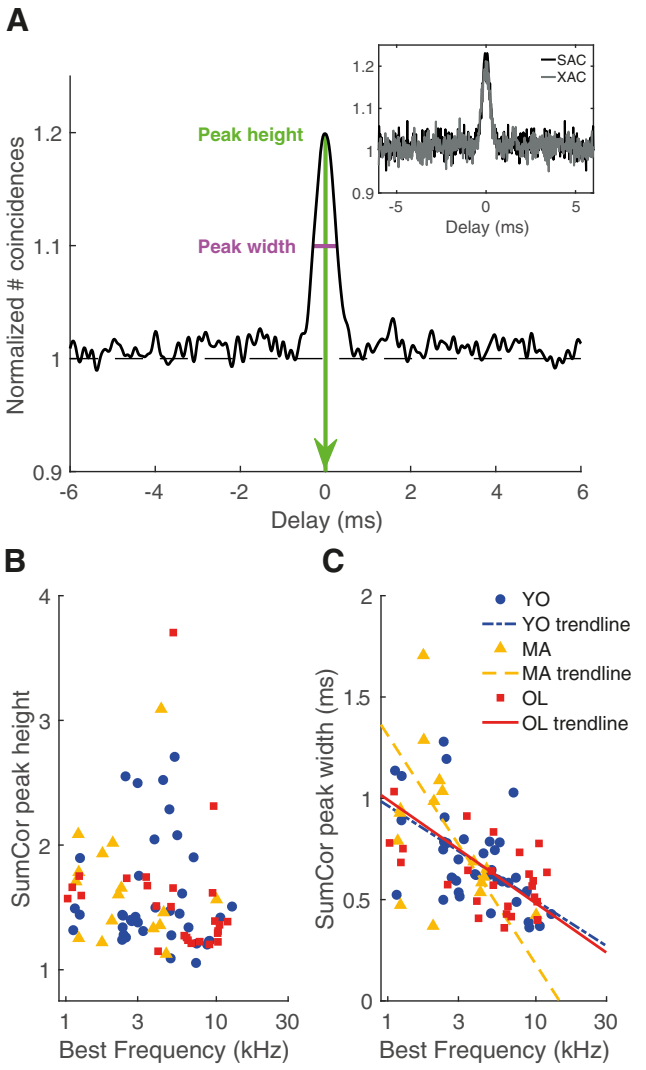

Figure 6. SumCor peak height and width were not affected by aging. ***A***, Example of the SumCor of a unit of a young gerbil (BF = 7.5 kHz). Inset, The SAC and XAC of the same unit (XAC/SAC ratio = 1.02). Peak height (from 0) was 1.22 (green) and peak width was 0.53 ms (magenta). ***B***, SumCor peak height as a function of BF for young (blue circles; $n = 38$), middle-aged (yellow triangles; $n = 19$), and old gerbils (red squares; $n = 28$). ***C***, SumCor peak width as a function of BF for the different age groups. Logarithmic regressions are shown as visual aids.

Auditory nerve spontaneous firing rates were decreased with aging

SR was significantly decreased in ANFs of both middle-aged and old gerbils, compared with young gerbils (Kruskal–Wallis test: $H_{(2)} = 64.34$, $p = 1.07 \times 10^{-14}$; Mann–Whitney U tests: YO vs MA, $p = 4.50 \times 10^{-11}$, YO vs OL, $p = 5{,}90 \times 10^{-8}$, MA vs OL, $p = 0.15$; Fig. 7*A*). This difference between age groups was intriguing and prompted us to further differentiate between the low- and high-frequency parts of the cochlea. Separate Kruskal–Wallis tests showed that there was a significant effect of group in both the low- and the high-BF units (Kruskal–Wallis test: $H_{(2)} = 51.43$, $p = 6.79 \times 10^{-12}$, for fibers with a BF < 3.5 kHz; $H_{(2)} = 21.86$, $p = 1.79 \times 10^{-5}$, for fibers with a BF ≥ 3.5 kHz). *Post hoc* pairwise comparisons revealed a significant decrease of SR in low-BF units of the middle-aged and old animals (Mann–Whitney *U* tests: YO vs MA, $p = 6.04 \times 10^{-8}$, YO vs OL, $p = 1.22 \times 10^{-7}$, MA vs OL, $p = 0.64$; Fig. 7*C*) and a significant SR decrease in high-BF units in the middle-aged animals (Mann–Whitney *U* tests: YO vs MA, $p = 5.31 \times 10^{-5}$, YO vs OL, $p = 0.02$, MA vs OL, $p = 0.03$; Fig. 7*D*).

We wondered whether the decreased SR might reflect some association with age-related hearing loss, since the age of onset and the extent of age-related hearing loss were quite variable across different animals (Fig. 1*B*). Therefore, the SR was plotted as a function of the ABR threshold in response to chirps (Fig. 7*E*). Single-unit SRs negatively correlated with the individual's ABR threshold (Spearman's rank correlation: $\rho = -0.34$, $p = 1.70 \times 10^{-8}$), indicating that a larger extent of age-related hearing loss was accompanied by lower SRs in the single-unit auditory nerve fibers.

Tuning of auditory nerve fibers was not altered with aging

For a subset of units, we obtained receptive fields from which a frequency threshold curve, or tuning curve could be derived (Fig. 8*A*). From the tuning curve, $Q_{10\ dB}$ was calculated as a measure for tuning sharpness. $Q_{10\ dB}$ increased logarithmically with increasing CF for young, middle-aged, and old gerbils, but there was no significant difference in $Q_{10\ dB}$ between the different age groups (ANCOVA: effect of group, $F_{(2)} = 0.89$, $p = 0.42$; Fig. 8*B*). A second measure of ANF frequency tuning was derived from the frequency-response curves, where the bandwidth at the half-maximum rate was determined. Again, the log(bandwidth) correlated positively with log(BF), but no significant effect of group was observed ($F_{(2)} = 2.68$, $p = 0.07$; Fig. 8*C*). As a third measure, ANF tuning was derived from the spectrum of the *revcor* (Fig. 3*B*), which is commonly determined at 10 dB below the maximum magnitude and also represents frequency selectivity (Henry et al., 2016). Only units in which the *revcor* frequency corresponded to the BF (Fig. 3*D*) were analyzed for bandwidth. 10 dB bandwidth did not differ between the different groups (Kruskal–Wallis test: $H_{(2)} = 1.24$, $p = 0.54$; Fig. 8*D*). Note that estimated test power was low (<10%) for all three tuning metrics explored, such that we cannot exclude minor changes with age. However, as for similar cases above, the power estimates refer to the detectability of the very small differences that we actually observed and that are unlikely to have biological relevance (effect sizes <0.1). Together these data strongly suggest that, despite thresholds being increased in old gerbils, this did not affect tuning sharpness of their ANFs to a relevant degree.

Discussion

Our study demonstrated that temporal coding in ANFs of quiet-aged gerbils was not altered relative to young gerbils, at comparable sensation levels. This was shown using several different measures of temporal coding of responses to pure tones and to noise. Specifically, responses to noise revealed that both TFS and ENV coding remained unaffected in old gerbils. In addition, ANF SRs were significantly decreased, especially in low-frequency ANFs. Because these data were obtained from gerbils that were not exposed to noise damage or to any ototoxic events, the changes in spontaneous rates are likely the result of natural aging processes. This is further supported by the observation that despite elevated thresholds, ANF frequency tuning was not affected in middle-aged and old gerbils, in contrast to the typical loss of frequency tuning after noise trauma that causes a permanent threshold shift of similar magnitude (chinchilla; Henry et al., 2016).

Age-related temporal coding deficits likely arise central to the auditory nerve

Previous studies in animals judged to be of geriatric age for the respective species have shown temporal coding degradations at

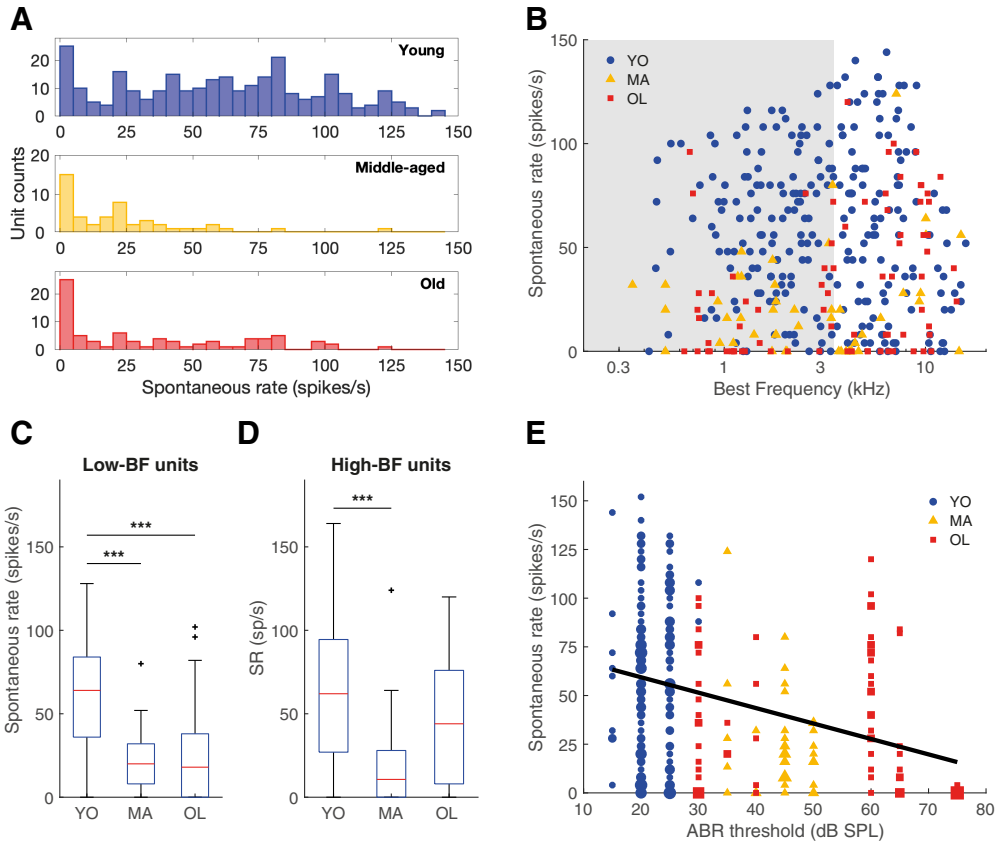

Figure 7. Auditory nerve SR decreased with age-related hearing loss. ***A***, The SR distribution of all auditory nerve single units recorded from young ($n = 272$; blue), middle-aged ($n = 48$; yellow), and old gerbils ($n = 78$; red). ***B***, SR plotted against BF in young (blue circles), middle-aged (yellow triangles), and old (red squares) animals. The gray shaded area indicates units with a BF < 3.5 kHz. ***C***, ***D***, Boxplots of SRs, separately for low-BF (***C***; YO: $n = 146$, MA: $n = 28$, OL: $n = 36$) and high-BF units (***D***; YO: $n = 137$, MA: $n = 20$, OL: $n = 44$), and for YO, MA, and OL gerbils in each graph. ***E***, SR plotted as a function of the ABR threshold to chirps of that animal (YO: $n = 149$, MA: $n = 37$, OL: $n = 78$). The black trend line represents the linear regression between ABR threshold and SR. Marker size represents the number of overlapping data points. $^{***}p < 0.001$. Outliers are presented as black crosses (+).

the level of the auditory brainstem (cochlear nucleus), midbrain (inferior colliculus), and cortex (Walton, 2010). Specifically, the minimal gap threshold is increased in the inferior colliculus (mice; Walton et al., 1998) and responses to amplitude modulated tones and noise are deteriorated in the dorsal cochlear nucleus (rats), inferior colliculus (mice), and primary auditory cortex (Rhesus macaque monkeys; Walton et al., 2002; Schatteman et al., 2008; Overton and Recanzone, 2016). Furthermore, humans with age-related hearing loss often present with deficits in various temporal processing tasks (Hopkins and Moore, 2011; Plack et al., 2014; Ozmeral et al., 2016). Therefore, it may seem surprising that temporal coding was not deteriorated in auditory-nerve single units of quiet-aged gerbils.

There are several possible explanations for this apparent discrepancy. First, temporal coding deficits central to the auditory nerve can be explained by a local age-related decrease in inhibition (Caspary et al., 1995; Gleich et al., 2003; Canlon et al., 2010; Rabang et al., 2012), and thus do not require any changes in the auditory-nerve input. Second, temporal coding deficits may develop, for example, at the endbulb of Held: the large axosomatic central synapse between ANFs and ventral cochlear nucleus neurons. The complexity of the endbulb of Held decreases with age in mice, even before thresholds are elevated (Muniak et al., 2018), corresponding to a functional decline of the synapse, as measured with patch-clamping (Xie, 2016; Xie and Manis, 2017). Last, the size of the ANF population, rather than the functional properties of the remaining individual units, may change as a function of age. Aging is associated with synaptopathy and neuropathy in mammals, i.e., a substantial decline in the number of inner hair cell–ANF synapses and spiral ganglion neurons, respectively (for reviews, see Liberman and Kujawa, 2017; Heeringa and Köppl, 2019). It is thought that the convergence of multiple ANFs on their postsynaptic targets in the cochlear nucleus contributes to enhanced phase locking in the auditory brainstem (Joris and Smith, 2008). Therefore, a decrease in ANF population size, as shown for the gerbil starting from 24–30 months of age (Keithley et al., 1989; Gleich et al., 2016), would be expected to affect temporal coding. Indeed, studies on envelope following responses (EFRs), which represent the electrophysiological responses of populations of brainstem and midbrain auditory neurons, showed decreased response amplitudes in aged rats and mice (Parthasarathy and Bartlett, 2011; Parthasarathy and Kujawa, 2018). When the sound level is matched for wave I amplitude, and thus activating equivalent numbers of ANFs (Parthasarathy and Kujawa, 2018), the effect of age is eliminated (Lai et al., 2017). Moreover, EFR amplitude also decreases following noise-induced synapse loss (Shaheen et al., 2015). Therefore, a decrease in auditory nerve population size, rather than degraded temporal coding abilities of single ANFs, may be the predominant peripheral contribution to central age-related temporal coding deficits.

Threshold loss combined with normal frequency tuning is consistent with age-related strial dysfunction

Quiet-aged gerbils present a mixture of strial presbyacusis and synaptopathy at 34–39 months of age, with minimal sensory presbycusis (Heeringa and Köppl, 2019). Elevated single-unit

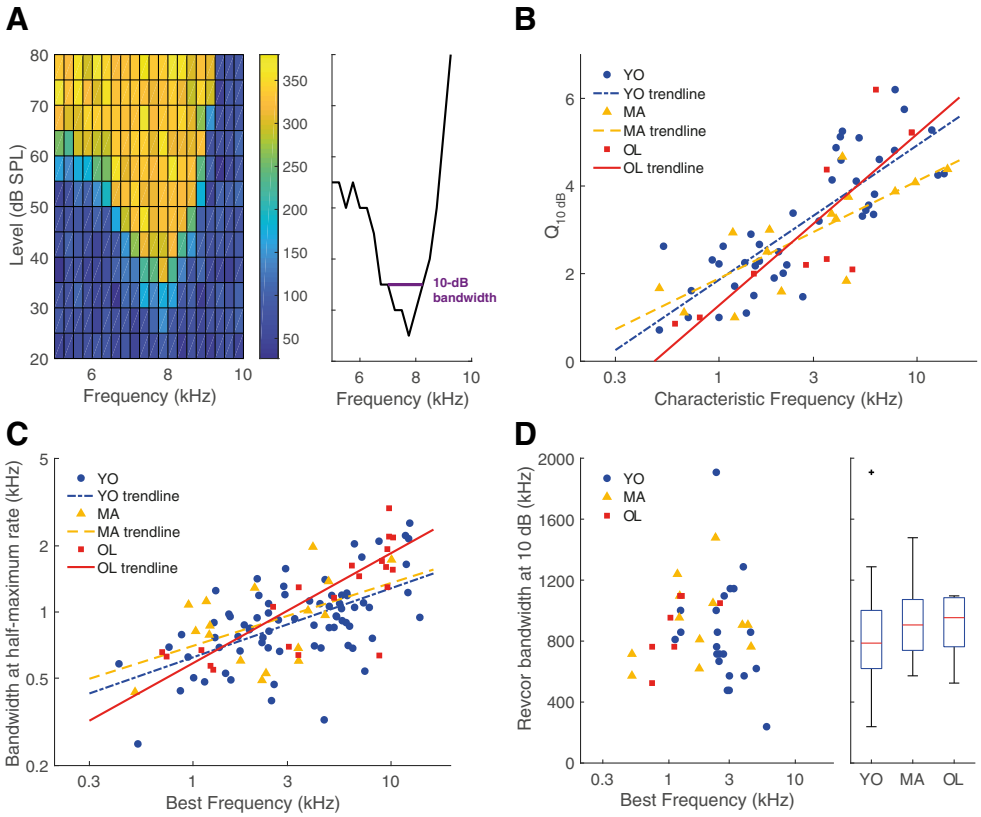

Figure 8. Frequency tuning of ANFs did not deteriorate with age. ***A***, Example of a receptive field (left) which shows the firing rate in spikes/s (mean over 50 ms stimulus) as a color code for all presented combinations of sound level (*y*-axis) and frequency (*x*-axis). From the receptive field, a tuning curve was derived (right), from which the $Q_{10\,dB}$ was calculated at 10 dB above threshold. ***B***, $Q_{10\,dB}$ as a function of CF. There was no difference between units recorded from young (blue circles; $n = 42$), middle-aged (yellow triangles; $n = 15$), and old gerbils (red squares; $n = 10$) but $Q_{10\,dB}$ generally increased with increasing CF. Exponential regression lines are shown as a visual aid. ***C***, Bandwidth of the iso-level response curve, at the half-maximum tone-evoked firing rate, shown in the same format as ***B*** (YO: $n = 75$, MA: $n = 17$, OL: $n = 22$). ***D***, Bandwidth of the *revcor* spectrum at 10 dB below the maximum magnitude, shown in the same format as ***B***. In addition, a boxplot shows the distribution of the *revcor* bandwidths for each group (YO: $n = 22$, MA: $n = 12$, OL: $n = 7$). Outliers are presented as black crosses (+).

and ABR thresholds are likely results of EP loss due to strial dysfunction (Schmiedt et al., 2002), which in turn affects cochlear amplification by outer hair cells (Ruggero and Rich, 1991). Consistently, experimentally induced EP loss, using furosemide injections, results in elevated single-unit and ABR thresholds (Sewell, 1984a; Schmiedt et al., 2002; Lang et al., 2010). In contrast, experimentally induced synaptopathy is typically not reflected in elevated thresholds; thresholds can remain normal in the face of synapse losses of up to 60% (Kujawa and Liberman, 2009; Bourien et al., 2014).

Despite elevated thresholds, tuning sharpness remained unaltered in ANFs of old gerbils. This is in marked contrast to noise-induced hearing loss, which is typically associated with broadened frequency selectivity and hypersensitivity of the low-frequency tuning-curve tail. Noise-induced hearing loss is associated predominantly with hair cell damage and loss (Liberman and Dodds, 1984), whereas hair-cell loss remains minimal in quiet-aged gerbils (Tarnowski et al., 1991). A recent study showed that auditory-nerve fiber's tip-to-tail ratios are much less affected in experimentally-induced strial dysfunction compared with noise-induced hearing loss of similar magnitude. Interestingly, the tip-to-tail ratio was likely the primary factor in temporal coding deficits accompanying the noise-induced hearing loss (Henry et al., 2019). Whereas noise trauma that causes permanent threshold shifts of similar magnitude as in our old gerbils resulted in enhanced temporal ENV coding, and distorted tonotopic coding of TFS and ENV (Kale and Heinz, 2010; Henry et al., 2016), these changes did not occur following experimentally-induced strial dysfunction with similar threshold shifts (Henry et al., 2019). In addition, experimentally-induced synaptopathy has no effect on auditory-nerve-fiber frequency tuning (Furman et al., 2013). Thus, the absence of both tuning deficits and temporal coding deficits are consistent with the typical pathologies in quiet-aged gerbils: strial dysfunction and synaptopathy (Heeringa and Köppl, 2019).

In summary, the single-unit phenotype of our quiet-aged gerbils, with threshold loss but unaltered frequency selectivity, is best explained by age-related strial dysfunction. Synaptopathy was likely present (Gleich et al., 2016) but is expected to affect neither threshold nor tuning measures.

Changes in spontaneous rates likely represent the mixed consequences of strial dysfunction and selective degeneration of fibers

Our study showed that SRs were decreased in both low- and high-frequency ANFs of quiet-aged gerbils and that this decrease was proportional to the extent of age-related hearing loss. A previous study on ANFs in quiet-aged gerbils (36–40 months old) found a reduced proportion of low-SR fibers (Schmiedt et al., 1996; Lang et al., 2010), apparently at odds with our results. However, this change was only significant for high-frequency ANFs (BFs > 6 kHz), with a trend in the opposite direction at lower BFs (Schmiedt et al., 1996). Thus, both studies agree on similar trends of decreased mean SRs at low

BFs in quiet-aged gerbils but found conflicting results for high-BF fibers that are currently unexplained.

ANFs are commonly classified based on their SR because it was shown that SR correlates with other fiber properties, both morphological and physiological, and thus defines two to three ANF types, depending on species (Heil and Peterson, 2015). The SR decrease observed in the present study may in principle be explained either by a specific loss of high-SR fibers or by a general reduction of SR in ANFs, leading to a change in individual fiber typology relative to that in young animals. It has been shown that furosemide-induced and hypoxia-induced EP loss decreases the SR of a unit (Manley and Robertson, 1976; Sewell, 1984b), suggesting a similar mechanism at work with age-related EP loss. In contrast to that, noise- and ouabain-induced synaptopathy is known to specifically target the low-SR fibers, resulting in an increase of mean SR (Furman et al., 2013; Bourien et al., 2014). Furthermore, in mice, spiral ganglion cells with the molecular signature of the likely low-SR type degenerate disproportionately as a function of age (Shrestha et al., 2018).

In summary, synaptopathy may specifically target low-SR fibers, whereas age-related EP loss may decrease the firing rates of remaining ANFs and blur the distinction of ANF types compared with young animals. The relative contributions of these two cochlear pathologies in a given animal, or even in different cochlear regions of the same animal, will then determine the distribution of spontaneous firing rates. Variable individual extents of synaptic loss and strial pathology in quiet-aged gerbils conceivably explain the minor conflicts between studies. Note that it is a common assumption that low-SR ANFs are crucial for signal-in-noise perception and that loss of the low-SR fibers thus results in problems with understanding speech in difficult listening conditions (Bharadwaj et al., 2014; Liberman, 2017). Recent papers have questioned this assumption and the relative importance of low- and high-SR fibers in complex auditory processing tasks is still under debate (Carney, 2018; Huet et al., 2018). Therefore, the consequences of age-related synaptopathy and reductions of intrinsic spontaneous rates in individual ANFs remain largely unknown.

References

Bharadwaj HM, Verhulst S, Shaheen L, Liberman MC, Shinn-Cunningham BG (2014) Cochlear neuropathy and the coding of supra-threshold sound. Front Syst Neurosci 8:26.

Bourien J, Tang Y, Batrel C, Huet A, Lenoir M, Ladrech S, Desmadryl G, Nouvian R, Puel JL, Wang J (2014) Contribution of auditory nerve fibers to compound action potential of the auditory nerve. J Neurophysiol 112:1025–1039.

Canlon B, Illing RB, Walton J (2010) Cell biology and physiology of the aging central auditory pathway. In: The aging auditory system (Gordon-Salant S, Frisina RD, Popper AN, Fay RR, eds), pp 39–74. New York: Springer.

Carney LH (2018) Supra-threshold hearing and fluctuation profiles: implications for sensorineural and hidden hearing loss. J Assoc Res Otolaryngol 19:331–352.

Caspary DM, Milbrandt JC, Helfert RH (1995) Central auditory aging: GABA changes in the inferior colliculus. Exp Gerontol 30:349–360.

Dau T, Wegner O, Mellert V, Kollmeier B (2000) Auditory brainstem responses with optimized chirp signals compensating basilar-membrane dispersion. J Acoust Soc Am 107:1530–1540.

de Boer E, de Jongh HR (1978) On cochlear encoding: potentialities and limitations of the reverse-correlation technique. J Acoust Soc Am 63:115–135.

de Boer R, Kuyper P (1968) Triggered correlation. IEEE Trans Biomed Eng 15:169–179.

FitzGerald JV, Burkitt AN, Clark GM, Paolini AG (2001) Delay analysis in the auditory brainstem of the rat: comparison with click latency. Hear Res 159:85–100.

Fitzgibbons PJ, Gordon-Salant S (1996) Auditory temporal processing in elderly listeners. J Am Acad Audiol 7:183–189.

Furman AC, Kujawa SG, Liberman MC (2013) Noise-induced cochlear neuropathy is selective for fibers with low spontaneous rates. J Neurophysiol 110:577–586.

Gates GA, Mills JH (2005) Presbycusis. Lancet 366:1111–1120.

Gleich O, Hamann I, Klump GM, Kittel M, Strutz J (2003) Boosting GABA improves impaired auditory temporal resolution in the gerbil. Neuroreport 14:1877–1880.

Gleich O, Semmler P, Strutz J (2016) Behavioral auditory thresholds and loss of ribbon synapses at inner hair cells in aged gerbils. Exp Gerontol 84:61–70.

Goldberg JM, Brown PB (1969) Response of binaural neurons of dog superior olivary complex to dichotic tonal stimuli: some physiological mechanisms of sound localization. J Neurophysiol 32:613–636.

Gordon-Salant S, Fitzgibbons PJ, Yeni-Komshian GH (2011) Auditory temporal processing and aging: implications for speech understanding of older people. Audiol Res 1:e4.

Gratton MA, Smyth BJ, Schulte BA, Vincent DA Jr (1995) Na, K-ATPase activity decreases in the cochlear lateral wall of quiet-aged gerbils. Hear Res 83:43–50.

Gurgel RK, Ward PD, Schwartz S, Norton MC, Foster NL, Tschanz JT (2014) Relationship of hearing loss and dementia: a prospective, population-based study. Otol Neurotol 35:775–781.

Heeringa AN, Köppl C (2019) The aging cochlea: towards unraveling the functional contributions of strial dysfunction and synaptopathy. Hear Res 376:111–124.

Heil P, Peterson AJ (2015) Basic response properties of auditory nerve fibers: a review. Cell Tissue Res 361:129–158.

Heil P, Peterson AJ (2017) Spike timing in auditory-nerve fibers during spontaneous activity and phase locking. Synapse 71:5–36.

Heil P, Neubauer H, Irvine DR, Brown M (2007) Spontaneous activity of auditory-nerve fibers: insights into stochastic processes at ribbon synapses. J Neurosci 27:8457–8474.

Heinz MG, Swaminathan J (2009) Quantifying envelope and fine-structure coding in auditory nerve responses to chimaeric speech. JARO 10:407–423.

Hellstrom LI, Schmiedt RA (1991) Rate/level functions of auditory-nerve fibers in young and quiet-aged gerbils. Hear Res 53:217–222.

Henry KS, Kale S, Heinz MG (2016) Distorted tonotopic coding of temporal envelope and fine structure with noise-induced hearing loss. J Neurosci 36:2227–2237.

Henry KS, Sayles M, Hickox AE, Heinz MG (2019) Divergent auditory nerve encoding deficits between two common etiologies of sensorineural hearing loss. J Neurosci 39:6879–6887.

Hopkins K, Moore BC (2007) Moderate cochlear hearing loss leads to a reduced ability to use temporal fine structure information. J Acoust Soc Am 122:1055–1068.

Hopkins K, Moore BC (2011) The effects of age and cochlear hearing loss on temporal fine structure sensitivity, frequency selectivity, and speech reception in noise. J Acoust Soc Am 130:334–349.

Huet A, Batrel C, Tang Y, Desmadryl G, Wang J, Puel JL, Bourien J (2016) Sound coding in the auditory nerve of gerbils. Hear Res 338:32–39.

Huet A, Desmadryl G, Justal T, Nouvian R, Puel JL, Bourien J (2018) The interplay between spike-time and spike-rate modes in the auditory nerve encodes tone-in-noise threshold. J Neurosci 38:5727–5738.

Joris PX (2003) Interaural time sensitivity dominated by cochlea-induced envelope patterns. J Neurosci 23:6345–6350.

Joris PX, Smith PH (2008) The volley theory and the spherical cell puzzle. Neuroscience 154:65–76.

Joris PX, Louage DH, Cardoen L, van der Heijden M (2006) Correlation index: a new metric to quantify temporal coding. Hear Res 216–217:19–30.

Kale S, Heinz MG (2010) Envelope coding in auditory nerve fibers following noise-induced hearing loss. J Assoc Res Otolaryngol 11:657–673.

Keine C, Rübsamen R (2015) Inhibition shapes acoustic responsiveness in spherical bushy cells. J Neurosci 35:8579–8592.

Keithley EM, Ryan AF, Woolf NK (1989) Spiral ganglion cell density in young and old gerbils. Hear Res 38:125–133.

Kujawa SG, Liberman MC (2009) Adding insult to injury: cochlear nerve degeneration after "temporary" noise-induced hearing loss. J Neurosci 29:14077–14085.

Kujawa SG, Liberman MC (2015) Synaptopathy in the noise-exposed and aging cochlea: primary neural degeneration in acquired sensorineural hearing loss. Hear Res 330:191–199.
Lai J, Sommer AL, Bartlett EL (2017) Age-related changes in envelope-following responses at equalized peripheral or central activation. Neurobiol Aging 58:191–200.
Lang H, Jyothi V, Smythe NM, Dubno JR, Schulte BA, Schmiedt RA (2010) Chronic reduction of endocochlear potential reduces auditory nerve activity: further confirmation of an animal model of metabolic presbyacusis. J Assoc Res Otolaryngol 11:419–434.
Liberman MC (2017) Noise-induced and age-related hearing loss: new perspectives and potential therapies. F1000Res 6:927.
Liberman MC, Dodds LW (1984) Single-neuron labeling and chronic cochlear pathology: III. Stereocilia damage and alterations of threshold tuning curves. Hear Res 16:55–74.
Liberman MC, Kujawa SG (2017) Cochlear synaptopathy in acquired sensorineural hearing loss: manifestations and mechanisms. Hear Res 349:138–147.
Lin FR, Thorpe R, Gordon-Salant S, Ferrucci L (2011) Hearing loss prevalence and risk factors among older adults in the united states. J Gerontol A Biol Sci Med Sci 66:582–590.
Louage DH, van der Heijden M, Joris PX (2004) Temporal properties of responses to broadband noise in the auditory nerve. J Neurophysiol 91:2051–2065.
Manley GA, Robertson D (1976) Analysis of spontaneous activity of auditory neurons in spiral ganglion of guinea-pig cochlea. J Physiol 258:323–336.
Mardia KV, Jupp PE (2000) Directional statistics. New York:Wiley.
Muniak MA, Ayeni FE, Ryugo DK (2018) Hidden hearing loss and endbulbs of held: evidence for central pathology before detection of ABR threshold increases. Hear Res 364:104–117.
Overton JA, Recanzone GH (2016) Effects of aging on the response of single neurons to amplitude-modulated noise in primary auditory cortex of rhesus macaque. J Neurophysiol 115:2911–2923.
Ozmeral EJ, Eddins AC, Frisina DR Sr, Eddins DA (2016) Large cross-sectional study of presbycusis reveals rapid progressive decline in auditory temporal acuity. Neurobiol Aging 43:72–78.
Parthasarathy A, Bartlett EL (2011) Age-related auditory deficits in temporal processing in F-344 rats. Neuroscience 192:619–630.
Parthasarathy A, Kujawa SG (2018) Synaptopathy in the aging cochlea: characterizing early-neural deficits in auditory temporal envelope processing. J Neurosci 38:7108–7119.
Plack CJ, Barker D, Prendergast G (2014) Perceptual consequences of "hidden" hearing loss. Trends Hear 18:1–11.
Rabang CF, Parthasarathy A, Venkataraman Y, Fisher ZL, Gardner SM, Bartlett EL (2012) A computational model of inferior colliculus responses to amplitude modulated sounds in young and aged rats. Front Neural Circuits 6:77.
Recio-Spinoso A, Temchin AN, van Dijk P, Fan YH, Ruggero MA (2005) Wiener-kernel analysis of responses to noise of chinchilla auditory-nerve fibers. J Neurophysiol 93:3615–3634.
Rosen S (1992) Temporal information in speech: acoustic, auditory and linguistic aspects. Philos Trans R Soc Lond B Biol Sci 336:367–373.
Ruggero MA, Rich NC (1991) Furosemide alters organ of corti mechanics: evidence for feedback of outer hair cells upon the basilar membrane. J Neurosci 11:1057–1067.
Schatteman TA, Hughes LF, Caspary DM (2008) Aged-related loss of temporal processing: altered responses to amplitude modulated tones in rat dorsal cochlear nucleus. Neuroscience 154:329–337.
Schmiedt RA (1993) Cochlear potentials in quiet-aged gerbils: does the aging cochlea need a jump start? In: Sensory research: multimodal perspectives. (Verrillo RT, ed), pp 91–103. Hillsdale, NJ: Lawrence Erlbaum.
Schmiedt RA (1996) Effects of aging on potassium homeostasis and the endocochlear potential in the gerbil cochlea. Hear Res 102:125–132.
Schmiedt RA, Mills JH, Boettcher FA (1996) Age-related loss of activity of auditory-nerve fibers. J Neurophysiol 76:2799–2803.
Schmiedt RA, Lang H, Okamura HO, Schulte BA (2002) Effects of furosemide applied chronically to the round window: a model of metabolic presbyacusis. J Neurosci 22:9643–9650.
Schuknecht HF, Gacek MR (1993) Cochlear pathology in presbycusis. Ann Otol Rhinol Laryngol 102:1–16.
Schulte BA, Schmiedt RA (1992) Lateral wall na, K-ATPase and endocochlear potentials decline with age in quiet-reared gerbils. Hear Res 61:35–46.
Sergeyenko Y, Lall K, Liberman MC, Kujawa SG (2013) Age-related cochlear synaptopathy: an early-onset contributor to auditory functional decline. J Neurosci 33:13686–13694.
Sewell WF (1984a) The effects of furosemide on the endocochlear potential and auditory-nerve fiber tuning curves in cats. Hear Res 14:305–314.
Sewell WF (1984b) The relation between the endocochlear potential and spontaneous activity in auditory nerve fibres of the cat. J Physiol 347:685–696.
Shaheen LA, Valero MD, Liberman MC (2015) Towards a diagnosis of cochlear neuropathy with envelope following responses. J Assoc Res Otolaryngol 16:727–745.
Shannon RV, Zeng FG, Kamath V, Wygonski J, Ekelid M (1995) Speech recognition with primarily temporal cues. Science 270:303–304.
Shrestha BR, Chia C, Wu L, Kujawa SG, Liberman MC, Goodrich LV (2018) Sensory neuron diversity in the inner ear is shaped by activity. Cell 174:1229–1246.e17.
Strawbridge WJ, Wallhagen MI, Shema SJ, Kaplan GA (2000) Negative consequences of hearing impairment in old age: a longitudinal analysis. Gerontologist 40:320–326.
Swaminathan J, Mason CR, Streeter TM, Best V, Roverud E, Kidd G Jr (2016) Role of binaural temporal fine structure and envelope cues in cocktail-party listening. J Neurosci 36:8250–8257.
Tarnowski BI, Schmiedt RA, Hellstrom LI, Lee FS, Adams JC (1991) Age-related changes in cochleas of Mongolian gerbils. Hear Res 54:123–134.
Versteegh CP, Meenderink SW, van der Heijden M (2011) Response characteristics in the apex of the gerbil cochlea studied through auditory nerve recordings. J Assoc Res Otolaryngol 12:301–316.
Walton JP (2010) Timing is everything: temporal processing deficits in the aged auditory brainstem. Hear Res 264:63–69.
Walton JP, Frisina RD, O'Neill WE (1998) Age-related alteration in processing of temporal sound features in the auditory midbrain of the CBA mouse. J Neurosci 18:2764–2776.
Walton JP, Simon H, Frisina RD (2002) Age-related alterations in the neural coding of envelope periodicities. J Neurophysiol 88:565–578.
Xie R (2016) Transmission of auditory sensory information decreases in rate and temporal precision at the endbulb of held synapse during age-related hearing loss. J Neurophysiol 116:2695–2705.
Xie R, Manis PB (2017) Synaptic transmission at the endbulb of held deteriorates during age-related hearing loss. J Physiol 595:919–934.